The International Journal of Advanced Manufacturing Technology (2023) 128:1243–1254
https://doi.org/10.1007/s00170-023-11999-6

ORIGINAL ARTICLE

Friction plug-riveting spot welding process of steel/aluminum dissimilar materials and the joint formation mechanism

Jianyu Li[1] · Yajia Liu[1] · Shuai Gong[1] · Shuhai Chen[1] · Jian Yang[1] · Jihua Huang[1] · Shujun Chen[2] · Xiaoqing Jiang[2]

Received: 14 March 2023 / Accepted: 17 July 2023 / Published online: 25 July 2023
© The Author(s), under exclusive licence to Springer-Verlag London Ltd., part of Springer Nature 2023

Abstract

The welding characteristics of 7075 aluminum alloy and DP980 dual-phase steel sheet were systematically studied by the friction plug-riveting spot welding technology. The effects of different welding parameters on the weld formation, tensile strength, and microstructure of welded joints were analyzed. The complete metallurgical joining interface was formed between the rivet and steel plate. A partial metallurgical joining interface was formed between the circumferential surface of the rivet shaft and the aluminum alloy close to the steel sheet. However, the position of the rivet head did not form a metallurgical joining with the aluminum alloy. During the welding process, the area of the rivet interface underwent severe plastic deformation by frictional heat and down pressure; thus, there was a violent interaction between the plastically deformed metal and the surrounding aluminum alloy. The molten aluminum infiltrated into the rivet at the most of sample joints. The penetration of aluminum had a negative effect on the shear load. The maximum shear load of the joint was 14.374 kN. There were two types of fractures: the internal fracture of the rivet and the fracture of the steel/steel friction interface. When the fracture mode was an internal fracture of the rivet, the shear load was generally greater than the steel/steel friction interface.

Keywords 7075 aluminum alloy · DP980 steel · Spot joining · Intermetallic compound · Mechanical properties

1 Introduction

In the twenty-first century, the design of structural parts has been put forward at higher demand in the field of aerospace, aviation, and automobile industries. Now, it has become a hot topic. Recently, Al alloys have been used widely in body manufacture. Even a whole aluminum body was used to achieve lightweight in some high-end car brands, such as BMW 5 Series, Weilai ES8, and Audi A8. Currently, with the growing use of Al alloys, advanced high-strength steel was designed into automotive structures because they have the best comprehensive performance combined with moderate price. Hence, lightweight vehicles reduce tail gas emissions to achieve energy savings. However, the challenge of welding AA/AHSS will inevitably be encountered in the hybrid automotive body structure industry.

There is no doubt that there are enormous differences in the physical and chemical properties of steel/aluminum materials. Yang et al. [1] joined steel to aluminum joints made using fusion-based techniques, which typically have poor mechanical qualities. In a related investigation by Ma et al. [2], the intermetallic compound layers with different thicknesses can be obtained by changing the heat input. Li et al. [3] observed the formation of multiple intermetallic compounds in the welded joints. The most tricky question was that a series of intermetallic compounds would be generated by fusion welding.

At present, the traditional resistance spot welding technology had been widely used in body manufacturing. However, Al alloy joining to ultra-high-strength steel was difficult with this technique. Qiu et al. [4] indicated that the intermetallic compounds have an obvious impact on the tensile shear strength of the A5052/SPCC joint. Azhari-Saray et al. [5] reported that the visible interface was formed on the Al/HEA side. Chen et al. [6] found that the thickness of IMC was the main factor affecting the failure mode and mechanical properties of joints, though the thickness of IMCs was effectively

✉ Shuhai Chen
shchen@mater.ustb.edu.cn; shchenhit@gmail.com

[1] School of Materials Science and Engineering, University of Science and Technology Beijing, Beijing 100083, People's Republic of China

[2] The College of Mechanical Engineering and Applied Electronics Technology, Beijing University of Technology, Beijing 100124, People's Republic of China

shrunk by adjusting the conditions. In essence, the resistance spot welding is subordinate to fusion welding. So, the intermetallic compounds can not be completely eliminated. Except that, the self-piercing riveting (SPR) technology also plays an important role in body manufacturing. Karathanasopoulos et al. [7] found that the joint quality depends on the rivet leg thickness and mold depth. When the value of a high tensile strength steel plate is lower than 500 MP, Abe et al. [8] found that high-quality joints with aluminum alloy plates can be achieved by using traditional self-piercing technology. Mori et al. [9] reported that the joining range for self-piece riveting can be expanded by optimizing the shape of the die. Karathanasopoulos and Mohr [10] found that the use of high-strength rivets and bottom sheet is conducive to increasing the peel strength of joints. Similarly, there are some limitations for metal materials with a strength higher than 800 MPa.

As a solid-state welding, friction stir spot welding is one of the representative methods. Because the heat input is lower than the melting point of the base metal, the formation of intermetallic compounds can be avoided effectively. Li et al. [11] reported that the mechanical properties of the joint can be significantly improved when the sleeve downforce mode is used. Compared with the traditional FSSW joint, the strength of the joint obtained by the keyhole-refilled friction stir welding method is increased by 56.33% [12]. When the material is non-coated mild steel, Takeoka et al. [13] found that scrubbing refilled friction stir spot welding technology has more advantages than traditional FSSW technology, which can obtain a higher joint load. Yu et al. [14] found that the thickness of the intermetallic compound layer increased as the sleeve distance, and the maximum shear strength value is 7.31 kN. However, traditional friction stir spot welding leaves a keyhole at the joint which brings many unfavorable consequences. On this basis, the stirring head was optimized and transformed. The keyhole-free joint was realized by the relative movement between the pin and sleeve.

In response to the problems of the above methods, a new approach of solid-state spot welding method has been posted and developed in recent years. The friction bit joining (FBJ) is also known as friction unit welding or friction element welding. This method is developed by combining the principles of tribology and mechanical fastening. In this study, it is called friction plug-riveting spot welding technology. Huang et al. [15] found that the joint interface was divided into three regions: separation interface region, partial metallurgical bonding region, and complete metallurgical region depending on the degree of metallurgical bonding of materials. Miles et al. [16] reported that the joining interface between the rivet and the high-strength steel was the main source of joint strength. Furthermore, Miles et al. [17] identified that the flat design can obtain a higher lap shear strength, but the stability of the fluted design is better than the flat design. Lim et al. [18] discussed that the GA coating layer on steel plates can greatly improve corrosion resistance. With the increasing number of corrosion cycles, Lim et al. [19] found that the joint strength of specimens without adhesive decreased significantly. Squires et al. [20] pointed out that an adhesive with a thickness of up to 500 mm can increase the tensile load by 50%. Although friction plug-riveting spot welding has made certain research progress, there are still many gaps in the research on the formation mechanism of joints and the influence of welding parameters on the microstructure and performance of the joint. Revealing the interaction mechanism between the riveted metal and the Al alloy near the friction interface has important significance to enhance the joint quality.

In this study, the welding characteristics of 7075 aluminum alloy and DP980 dual-phase steel were systematically studied by the friction plug-riveting spot welding technology. The influence of welding process parameters on the joint formation, microstructure, and mechanical properties was investigated, and the relationship between the joint formation mechanism, microstructure, and mechanical properties was discussed.

2 Experimental procedure

2.1 Experimental materials

The base materials were 2-mm-thick 7075 and 1-mm-thick DP980. The microstructure of DP 980 was composed of 60% martensite and 40% ferrite with a nominal ultimate tensile strength of 980 MPa. The joining bits were made from 1045 steel. All sheets were cut into coupons with dimensions of 39 mm in width and 125 mm in length with an overlap of 39 mm in the joint area. The nominal chemical compositions of the material are given in Table 1. The mechanical properties of the base material are shown in Table 2. Figure 1 shows the schematic diagram of the structure and size of the rivet.

The structure of the bit needs to meet the following requirements: (1) The bit can drill well through the top layer (or layers) of material. In this work, the tip of the rivet was designed to be a tapered structure that can concentrate pressure on a point. This design was conducive to crushing the aluminum in a state of thermoplastic state and extruding the aluminum circumferentially; (2) the upper part of the rivet must cover the extruded aluminum. Therefore, the head of the rivet was designed with a hat-shaped groove, which can not only cover the aluminum well but improve the cleanliness of the workpiece surface. In all configurations, the aluminum sheet was on the top, while the steel sheets were underneath.

Table 1 Chemical composition of DP 980, AA7075-T6, and 1045 (wt%)

Base	Chemical composition (wt%)												
	C	Mn	Si	Cr	S	P	Fe	Cu	Mg	Zn	Ti	Ni	Al
DP980	0.15	1.44	0.32	0.02	0.007	0.011	Bal.	-	-	-	-	-	-
AA7075-T6	-	0.3	0.4	0.18–0.28	-	-	0.5	1.2–2	2.1–2.9	5.1–6.1	0.2	-	Bal.
1045	0.43–0.5	0.6–0.9	0.17–0.37	0.25	0.035	0.035	Bal.	0.25	-	-	-	0.25	-

Table 2 Mechanical properties of test materials

Base	Yield strength (MPa)	Tensile strength (MPa)	Elongation (%)
DP980	703	1009	16
AA7075-T6	462	524	11
1045	355	600	16

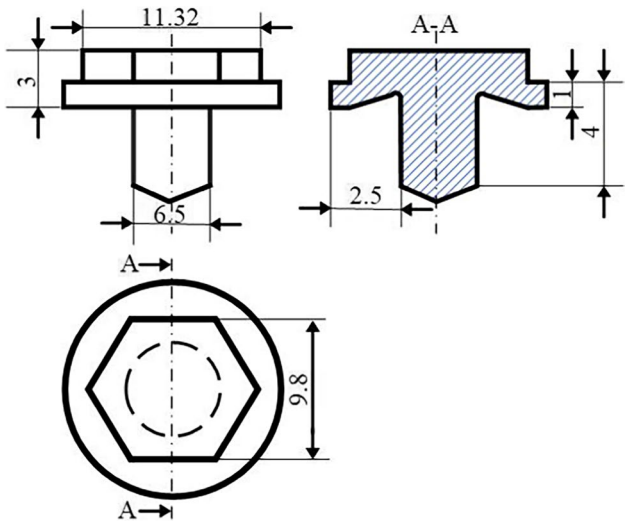

Fig. 1 Schematic diagram of the structure and size of the rivet

2.2 Materials and methods

Figure 2 shows the appearance of friction plug-riveting spot welding equipment. The welding structure mainly consists of rotary motion components, axial motion components, chucks, servo motors, sensors, and so on. The end face of the rotating motion component was a mandrel shaft with a hexagonal groove. Furthermore, with the purpose of attracting the rivet, a laminated magnet was placed in the groove. The rotational movement of the mandrel shaft was controlled by the rotary servo motor with a maximum speed of 4000 rpm/min. The axial movement of the spindle was controlled by the axial servo motor. The axial servo motor and ball screw were joined by the horizontal conveyor. The rotational motion of the axial servo motor was transmitted to the ball

Fig. 2 Friction plug-riveting spot welding machine

screw by the horizontal conveyor. The fixed plate on the ball screw was joined to the main shaft; thus, the ball screw can drive the main shaft to move axially. The grating scale was used to measure the axial displacement, and the measured result was fed back to the system to ensure the accuracy of axial displacement. At the same time, there was a pressure sensor in the middle of the chuck to measure the pressure during the welding process.

2.3 Metallographic characterization

The cross-sectioned joints were mounted and polished using different grades of abrasive paper (250, 400, 600, 800, 1200, 1500, and 2000). Finally, the rough-polished samples were continued to be polished with 1.5-mm diamond paste. An optical microscope and SEM were used to characterize the microstructures and macrostructure of the joints.

2.4 Experimental stage

Figure 3 is a schematic diagram of the friction plug-riveting spot welding process. The welding process could be divided into three stages. The first stage was the drilling

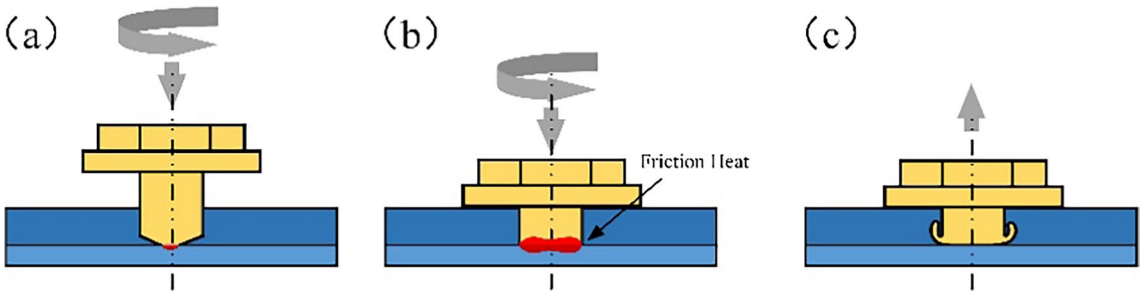

Fig. 3 Schematic diagram of friction plug-riveting spot welding process. **a** Hole turning stage. **b** Metallurgical stage. **c** Spindle parking and retraction stage

Table 3 A relevant table of parameters

Process parameters	Relevance to the process
RPM	Thermal input
Spindle pressing speed	Reaction time
Spindle depression depth	Solder joint diameter

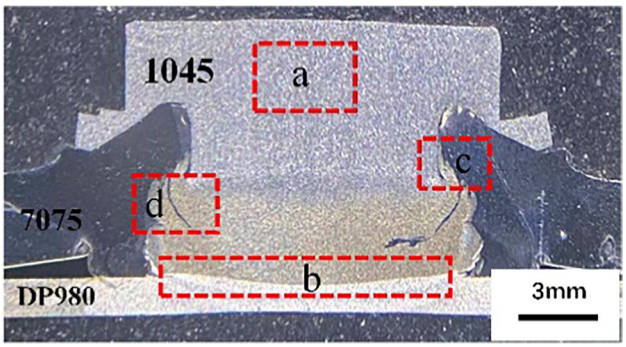

Fig. 4 Macroscopic topography of the joint cross-section

stage. This stage was performed invariably as the bit rotates at 2500 rpm/min and descends at a rate of 1.8 mm/s. The distance plunged by the bit was 2 mm. The second stage was the metallurgical stage when the bit cut through the top sheet. The joining bit was fed and rotated at a higher speed, and the bit continued to descend, causing frictional heating at the interface between the bit tip and bottom sheet. Thus, the steel was quickly turned into the thermoplastic state at the interface. The metallurgical bonding of rivets and steel plates was achieved. Furthermore, the rivets and the upper aluminum plate also form a mechanical bonding. The third stage was the retraction stage. After the joining was completed, the spindle of the welding machine was stopped very rapidly and then restarted to separate the joining bit from the weld, and the welding was completed. The entire process requires no surface preparation, pilot holes, or pre-drilling. Due to the elastic deformation of the equipment structure under high pressure, the actual welding displacement was less than the set displacement value.

The parameters of the drilling stage remain unchanged. The influence of process parameters was mainly studied in the metallurgical stage. The main goal of this study is to investigate the influence of process parameters on joint forming and mechanical properties (Table 3). The interaction mechanism between Al alloy, rivet, and steel sheet during the welding was revealed.

3 Results

3.1 Characteristics of the joints

Cross-sections of friction plug-riveting spot welded joint are shown in Fig. 4. During the processing, the joining bit was rotated at a speed of 3400 rpm and plunged into the sheet at 2.6 mm/s and the distance plunged by the bit was 3.6 mm. The friction plug-riveting composite spot welding joint consisted of three parts: rivet, 7075 aluminum alloy, and DP980. The hat-shaped rivet can well wrap the extruded aluminum alloy, which effectively improved the cleanliness of the workpiece surface. The upper layer of aluminum was bulged from the lower layer, which was far away from the location of the spot joint. The bulge was caused by the bit material between the joining layers during the welding cycle. Furthermore, the band-like structures appear on both sides of the rivet (Fig. 4d).

Figure 5 shows the microstructure of the friction plug-riveting spot welded joint. Figure 5a is the base metal of the rivet, consisting of ferrite and pearlite. Figure 5b is the interface between the steel plate and the rivet, and the lower part is the base metal of the steel plate, which consisted of ferrite matrix and martensite. Figure 5c is at the junction of the rivet with the aluminum alloy in the

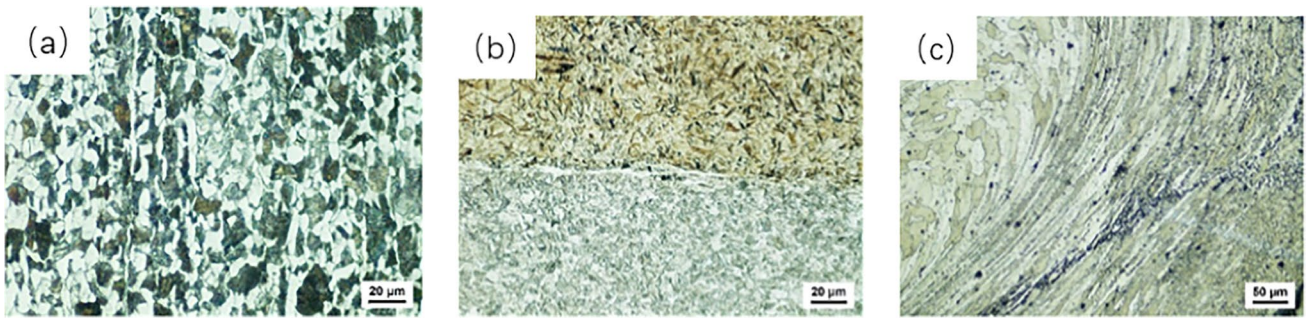

Fig. 5 Microstructure of the joint

circumferential direction with a streamlined structure. The aluminum alloy in the streamlined structure was formed by the extrusion of the "hook," and the circumferential friction was generated by the rotation of the rivet.

The microstructure of the rivet is enlarged, as shown in Fig. 6. No metallurgical joining is formed between the rivet head and aluminum, as shown in Fig. 6b. The bottom of the rivet underwent severe plastic deformation, which was extruded by the downforce. The violent interfacial reactions between extruded steel metal and aluminum alloy appeared to form a metallurgical connection, as shown in Fig. 6c. Figure 6d shows that these band-like structures contain a large number of aluminum components. Point A is mainly Fe-Al intermetallic compounds via an EDS elemental analysis with an atomic percentage of Fe/Al being 28.28:71.72; this phase is most likely Fe_2Al_5. Therefore, the band structure was formed because of the penetration of aluminum alloy into the rivet.

The microstructure of the outer edge of the interfacial region is shown in Fig. 6e. Some aluminum alloys were not fully extruded, which still exist in some areas between the rivet flash and steel plate, but aluminum alloy also reacts with the steel to form intermetallic compounds.

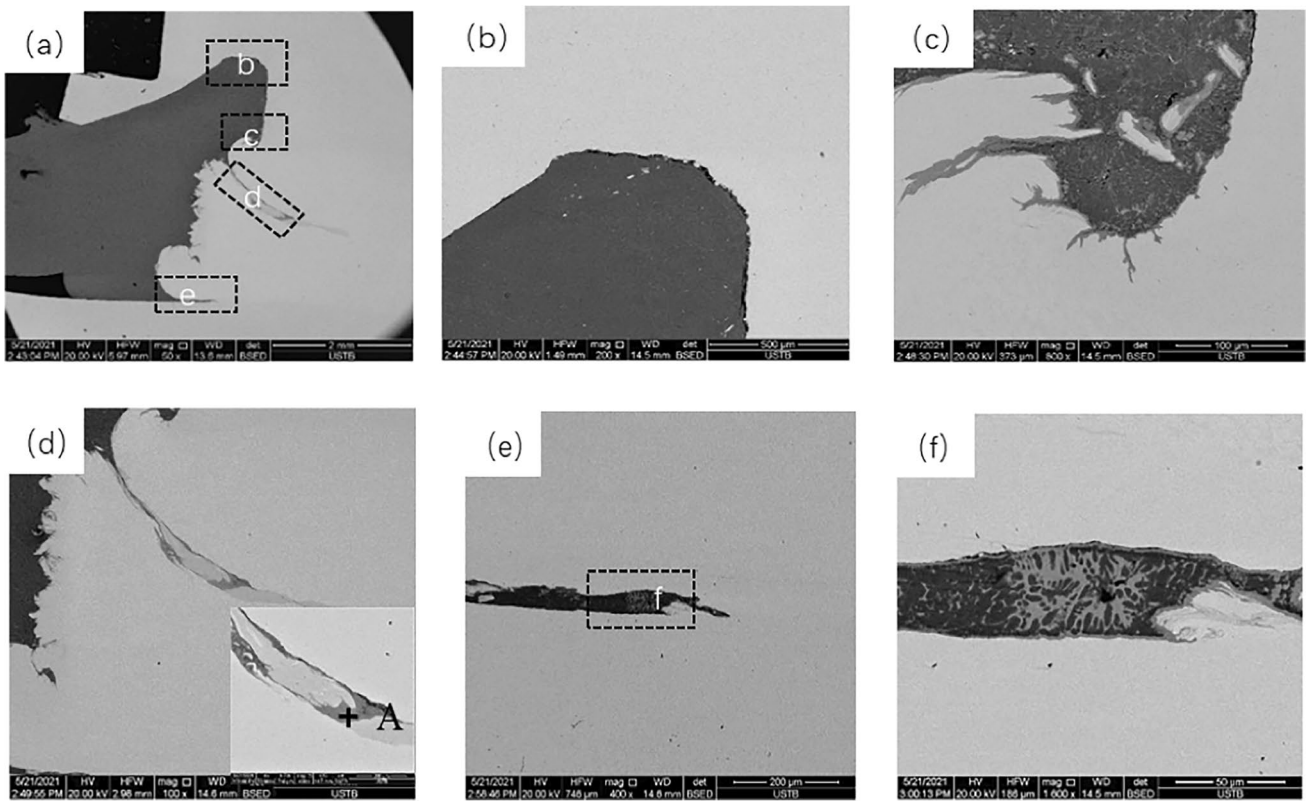

Fig. 6 Microscopic topography of the joint cross-section

To conclude, a complete friction welded interface was formed between the rivet and DP980 steel, which formed a complete metallurgical bonding. The severe plastic deformation metal in the circumferential direction of the rivet also has sufficient interface reaction with the Al aluminum; thus, a good metallurgical joining was formed. However, no metallurgical joining was formed in the area, where no noticeable plastic deformation occurred. Furthermore, a certain amount of aluminum alloy penetrated into the rivet by the complex reaction and thermal action, which would form a band-like structure.

3.2 Influence of process parameters on the joint forming

The macroscopic topography of the joint obtained at the different spindle depression depths is shown in Fig. 7 at a rotating speed of 3400 rpm and a plunge speed of 2.8 mm/s. The distance plunged by the bit was 2.8 mm, as shown in Fig. 7a; the filling state of the rivet head was not good, and the formability was poor. Simultaneously, no aluminum alloy was penetrated into the rivet to form a band-like structure. With the further increase of plunge distance, the phenomenon of the aluminum alloy infiltrating into the rivet appeared and the filling state of the rivet head was good.

Therefore, the penetration of the aluminum alloy was suppressed when the distance of plunged was small, but the formability was poor.

The macroscopic topography of the joint obtained at the different spindle rotation speeds is shown in Fig. 8 at the spindle pressing speed of 2.8 mm/s and the pressing amount of 3.6 mm. The joints were well joined, and the phenomenon of aluminum alloy infiltrating into the rivet occurred.

With the increase of the rotation speed, the position of the aluminum alloy infiltrating into the rivet has a downward flow trend. The increase of rotation speeds will sharply increase the circumferential frictional heat between the rivet and aluminum alloy and enhance the axial frictional extrusion heat between the rivet and steel plate. Because of the increased heat input, the volume of aluminum alloy will increase in the thermoplastic state, and the flowability of aluminum alloy also increases in the weld zone.

The rivet material at a high rotational speed made thinner layers of material to reach a thermoplastic state in a shorter time interval. At the thermal cycling conditions, thin layers of material were continuously stacked down with the rivet was pushed down continually. Therefore, the macroscopic performance has a downward flow trend where the aluminum alloy was penetrated into the rivet.

Figure 9 shows the macroscopic morphology of the joint at a rotation speed of 3400 rpm/min and a pressing distance of 3.6 mm, wherein the joints were well joined, and the phenomenon of aluminum alloy infiltrating into the rivet occurred. The influence of pressing speed was complex on the penetration, and the regularity was not noticeable.

3.3 Influence of process parameters on the tensile properties

The variation bar charts of tensile properties of welded joints at the different spindle depression depths are shown in Fig. 10 at a spindle rotation speed of 3400 rpm/min and a pressing speed of 2.8 mm/s.

With the increase of spindle depression depths, the shear load of the joint increased first and then decreased. The rivet head has poor filling and poor formability with the lowest joint shear load strength, and the shear load strength was 10.819 kN, and the amount of spindle depression depths was 2.8 mm. With the further increase of spindle depression depths, the contact area of the rivet with the steel/aluminum

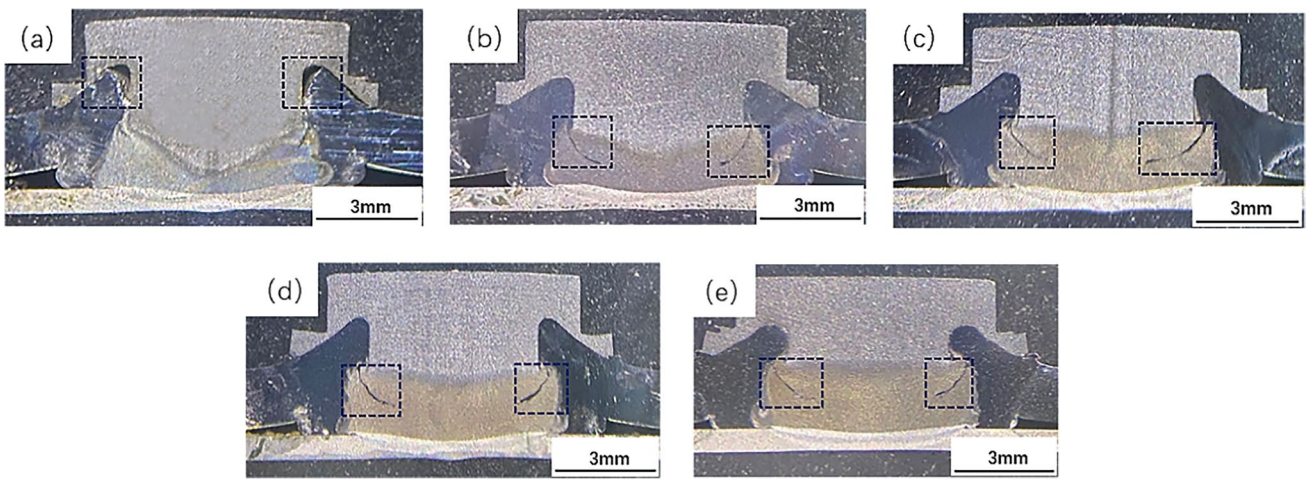

Fig. 7 Macro-morphology of joints under different spindle depression depths. **a** 2.8 mm. **b** 3.0 mm. **c** 3.2 mm. **d** 3.4 mm. **e** 3.6 mm

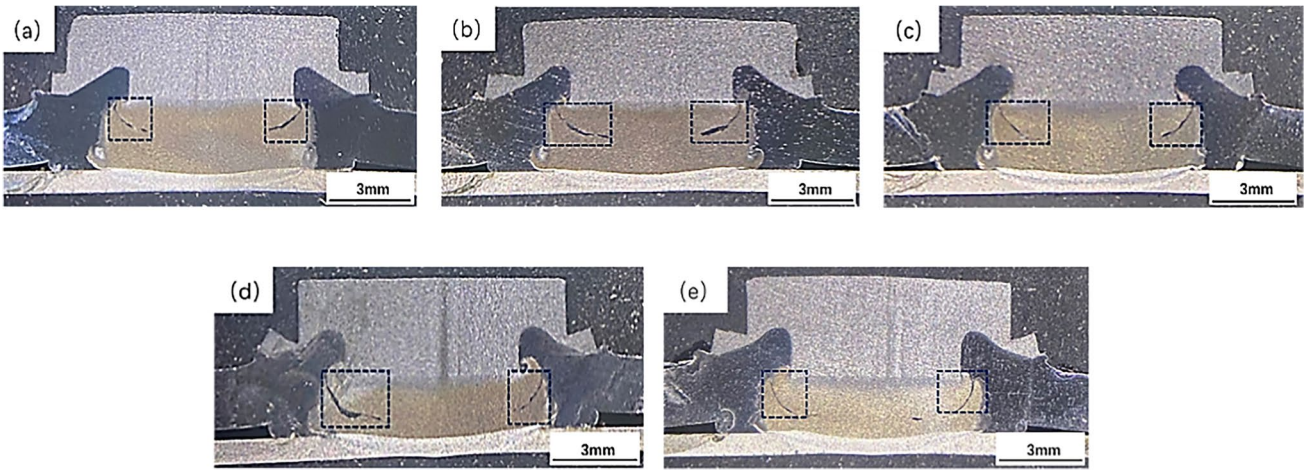

Fig. 8 Macro-morphology of the joint under different spindle rotation speeds. **a** 3000 rpm/min. **b** 3200 rpm/min. **c** 3400 rpm/min. **d** 3600 rpm/min. **e** 3800 rpm/min

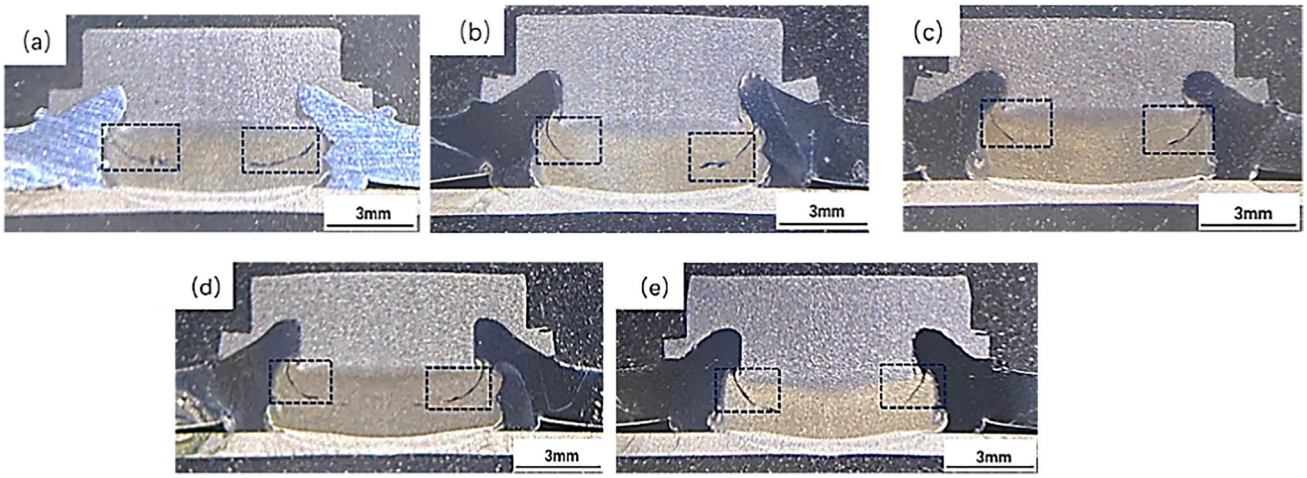

Fig. 9 Macro-morphology of the joint at the different spindle pressing speeds. **a** 2.4 mm/s. **b** 2.6 mm/s. **c** 2.8 mm/s. **d** 3.0 mm/s. **e** 3.2 mm/s

in both the axial and circumferential directions increased. Thus, the area of a metallurgical bond increased, which enhanced the shear load of the joint. The joint fracture location occurred at the frictional bonding interface between the rivet and steel plate. Therefore, the shear strength load of the joint was reduced at a pressing amount of 3.6 mm.

The variation bar charts of tensile properties of welded joints at the different spindle rotation speeds are shown in Fig. 11 at a spindle pressing speed of 2.8 mm/s and a spindle depression depth of 3.6 mm. With the increase of spindle rotational speed, the joint shear load decreased continuously. The shear load was the largest, and the maximum value was 14.374 kN at a spindle rotation speed of 3000 rpm/min.

As the rotational speed of the spindle increased, frictional heating raised, which intensified the interfacial reaction. Therefore, the fluidity of aluminum alloy was enhanced in this region. Because of the increase of spindle speed, the band-like structure appeared; thus, the shear strength of the joint decreased.

The variation bar charts of tensile properties of welded joints at the different spindle pressing speeds are shown in Fig. 12 at the spindle rotation speed of 3400 rpm/min and the spindle depression depths of 3.6 mm.

The results show that the pressing speed has a complex effect on the shear load of the joint. When the pressing speed was 2.4 mm/s, the welding time was relatively longer. The aluminum alloy has sufficient time to diffuse into the rivet, which can form a band-like structure. Thus, the shear load of the joint decreased. Simultaneously, the shear load strength of the joint was the smallest with a minimum value of 11.607 kN. With the further increase of pressing speed, the welding reaction time was greatly

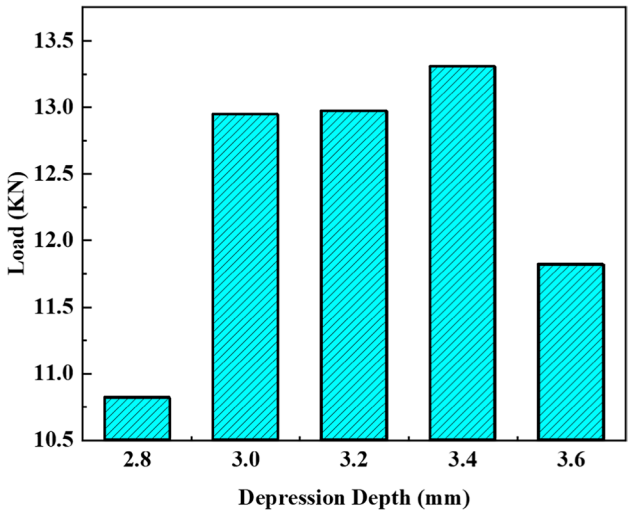

Fig. 10 Variation of the shear load of welded joints under different spindle depression depths

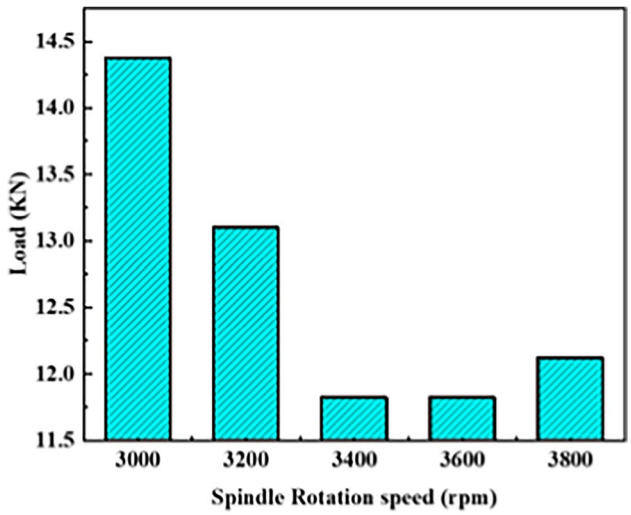

Fig. 11 Variation of the shear load of welded joints under different spindle rotation speeds

shortened. Therefore, the reaction time of aluminum alloy flowing into the rivet was reduced. The shear load strength of the joint was improved to a certain extent, and the joint load strength is 13.069 kN.

The strength calculation formula is $\sigma = \frac{N}{\mathrm{mm}^2} = \frac{14374N}{\pi r^2} = \frac{14374N}{\pi(3.25)^2} \approx 433$ MPa. The diameter of the rivet rod in the formula is 6.5 mm. While the tensile strength of 7075 aluminum alloy is about 524 MPa, the final calculation shows that the welding joint coefficient in this paper is 0.82, so the weld quality is reliable.

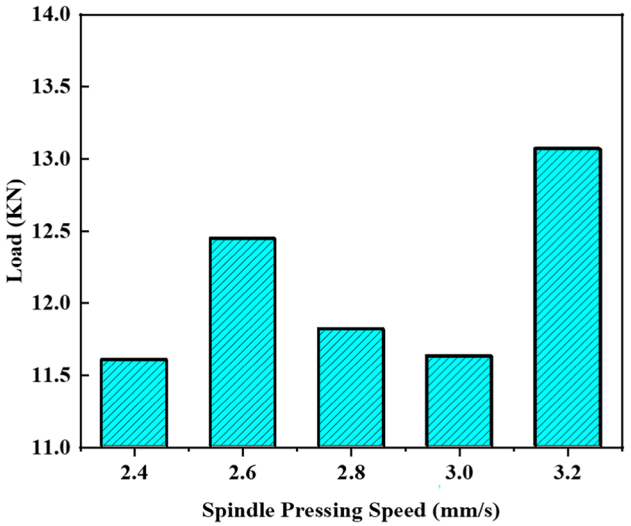

Fig. 12 Variation of the shear load of welded joints at the different spindle pressing speeds

3.4 Fracture analysis

It is seen that there were mainly two modes of fractures in the joint. The first fracture mode was the internal fracture of the rivet, as shown in Fig. 13a. The fracture position occurred in the rivet, and the remaining part was still tightly combined with the steel plate. The second fracture mode was broken from the friction interface, as shown in Fig. 13b. The lower end face of the rivet was completely separated from the lower steel plate. In this fracture mode, the metallurgical reaction between the rivet and the steel plate was insufficient. Thus, the joint strength was relatively low in this mode.

The two fracture modes of the joints are shown in Fig. 14. Figure 14a shows the fracture surface in the rivet. There are a large number of dimples in the fracture area of the joint, which are microscopically ductile fractures. Therefore, there was relatively higher fracture strength. Figure 14b shows the fracture surface in the steel/steel friction interface. The fracture presents a cleavage step with a river-like pattern, and the steps are along the same direction, exhibiting microscopically brittle fractures. Therefore, there was relatively lower fracture strength.

4 Discussions

4.1 Mechanism of aluminum infiltration

Figure 15 shows a schematic diagram of the aluminum infiltration process. Because the hardness and strength of the rivet were greater than the aluminum alloy, the rivet was in contact with the upper aluminum plate; the

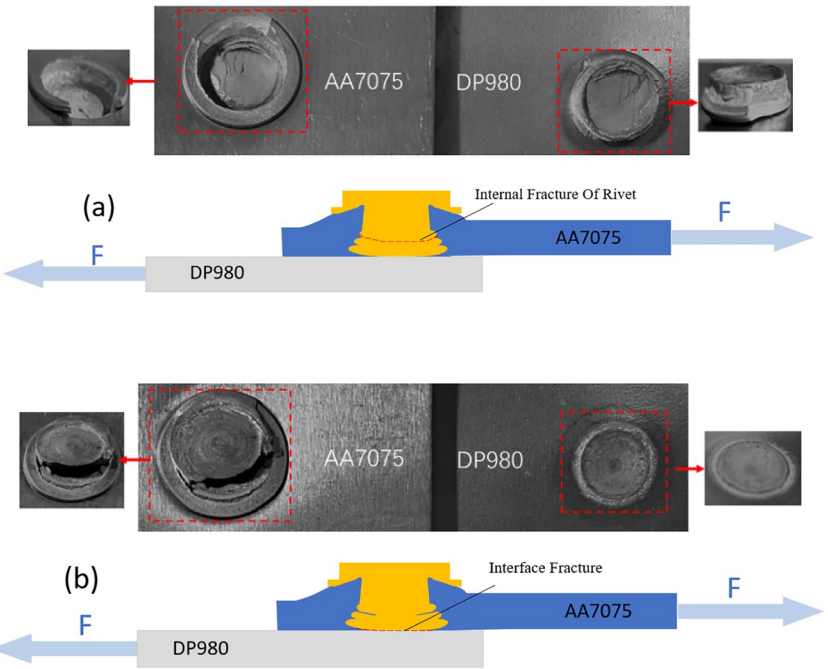

Fig. 13 Macroscopic fracture morphology and fracture form of the join. **a** Internal fracture of the rivet. **b** Interface fracture

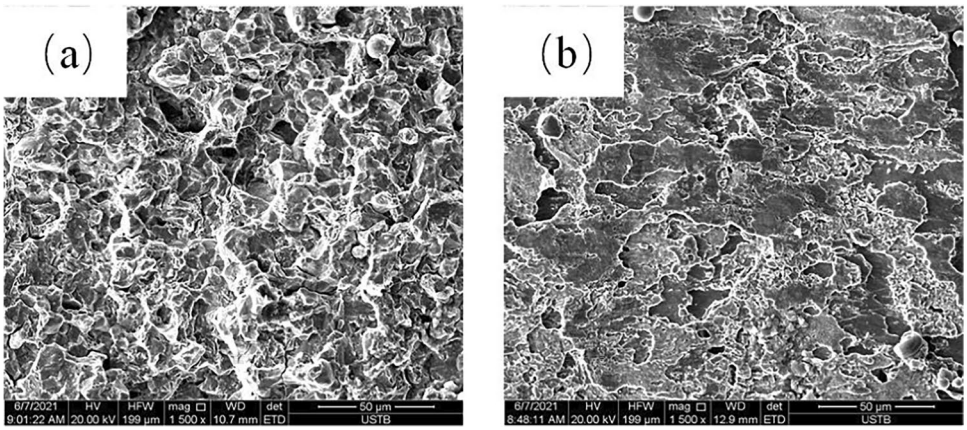

Fig. 14 Micromorphology of the fracture surface of the joint. **a** Internal fracture of the rivet. **b** Fracture of the steel/steel interface

aluminum alloy can quickly reach a thermoplastic state under the high-speed rotating rivet. Simultaneously, the aluminum alloy was continuously extruded around the rivet. When the rivet was in contact with the lower steel plate, the tip of the rivet was subjected to high stress and then induced plastic deformation. The plastic alloy was gradually extruded into the interface. At this stage, the friction linear velocity was not high due to the small diameter of the rivet tail. Therefore, the interface temperature was not high in this process, and aluminum alloy only underwent solid-state plastic deformation, as shown in Fig. 15b. As the aluminum alloy was continuously extruded, the temperature increased at the interface. Because the DP980 steel has higher strength and hardness than the rivet, the entire rivet was crushed in the high-temperature area, which induced a cake-like structure by the radial strain. Nevertheless, the DP980 steel basically does not have a noticeable plastic deformation, as shown in Fig. 15c. The peripheral linear velocity of the rivet was greater than the central linear velocity. As a result, the peripheral temperature of the rivet was higher than the central temperature. Therefore, the crushed and extruded metal reacted with the aluminum alloy at the interface and even melt the aluminum alloy at the interface.

With pressing the rivet, the plastic deformation metal of the rivet near the friction interface accumulated. As the pie structure continued to expand, the extruded metal reacted more violently with the aluminum alloy, as shown in Fig. 15d. After reaching a certain time and temperature, the metallurgical joining along the interface between the deformed pie metal and the DP980 steel began to form. As the interfacial friction proceeded, the metallurgical

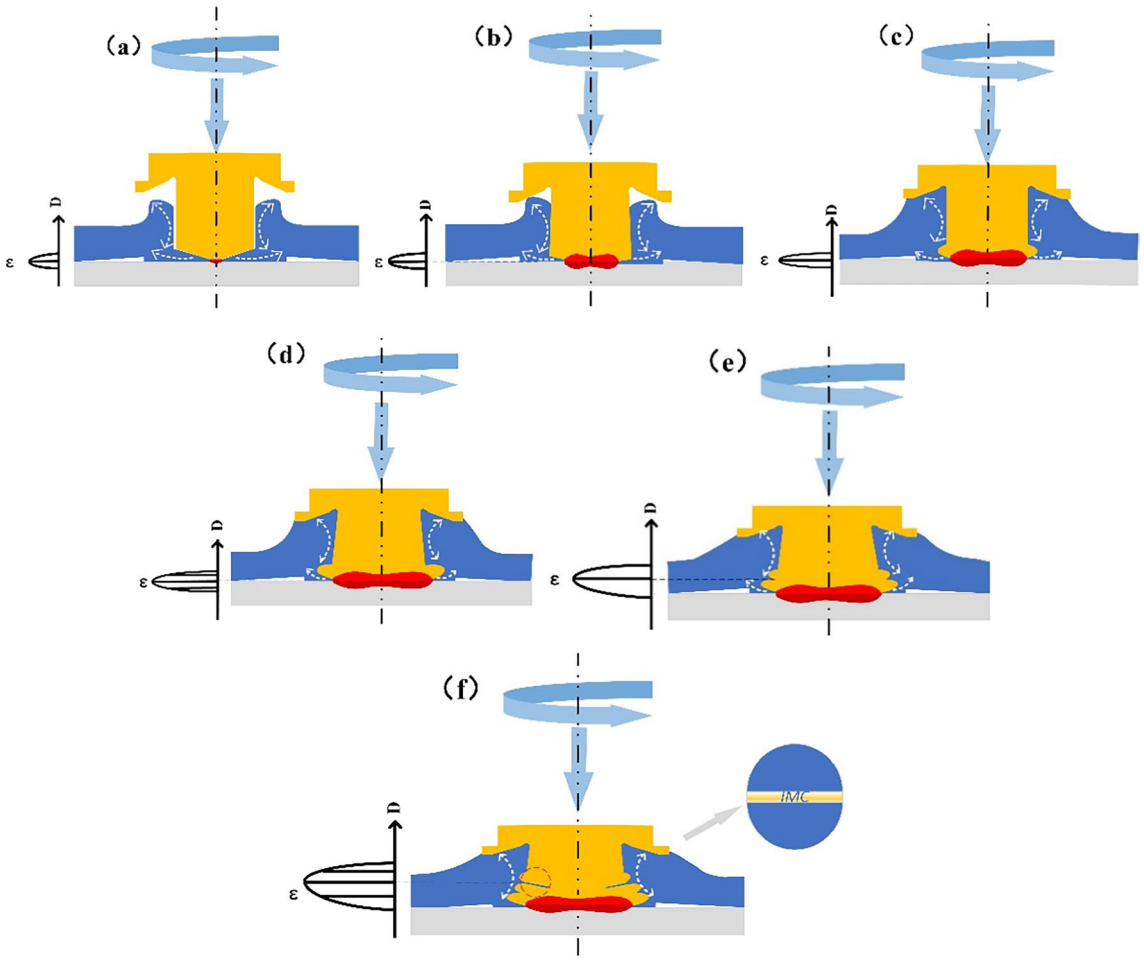

Fig. 15 Schematic diagram of the mechanism of aluminum infiltration

joining was intensified so that the joining strength increased between the pie and the DP980 steel. In addition, the deformed metal of the rivet accumulated along its axial direction, and then, the range of plastic deformation expands upward. The position of the peak tangential strain was shifted upwardly at the circumferential edge of the rivet because of the increase of frictional resistance. As a result, a new peak tangential strain zone was formed. With the increase of plastically deformed metal, a new pie-like structure was formed on the original pie-like structure during the continuous pressing of the rivet, as shown in Fig. 15e. As the friction process continues, it was possible to form multiple pie-like structures.

When the welding process was just completed, the interface temperature between the cake-like structure was relatively high. Thus, the aluminum alloy near to the cake-like structure was partially melted at the interface. Locally micro-melted aluminum alloys underwent interfacial reactions at the edges of the interface. Eventually, the intermetallic compound was formed. However, the tangential strain will not reach zero immediately between the final formed pie structure and rivet. The newly formed interface intermetallic compound was very brittle and has no ability to plastic deformation, which was torn. A small amount of molten aluminum alloy was penetrated into the interior of the torn crack as the process proceeded. The aluminum alloy continuously reacted with the fresh rivet material to form new intermetallic compounds. When the tangential strain decreased to zero, the micro-molten aluminum alloy solidified and the whole process was accomplished. Eventually, a band-like structure was formed, as shown in Fig. 15f.

4.2 Relationship between mechanical properties and aluminum infiltration

The band-like structure was composed of brittle intermetallic compounds, which has a negative effect on the mechanical properties of the joint. When the length of the band-like structure was longer, the mechanical properties of the

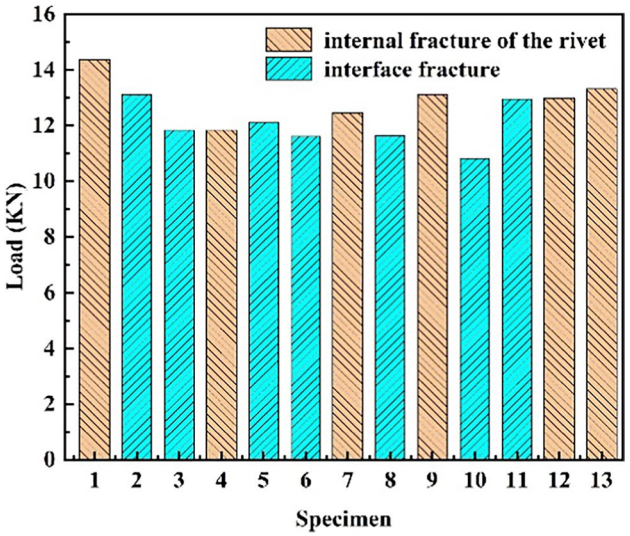

Fig. 16 Influence of fracture location on tensile shear strength

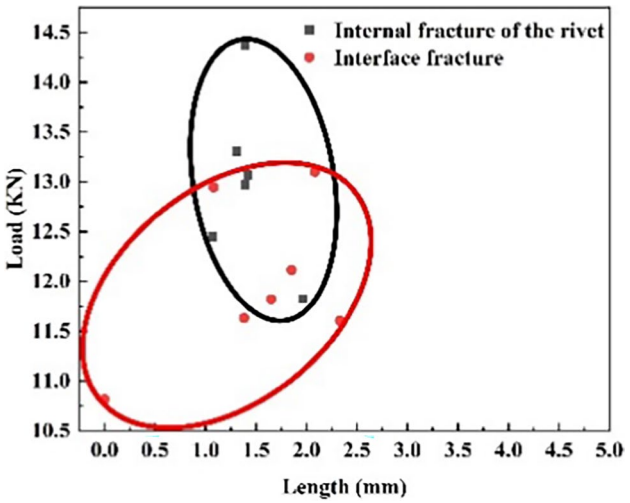

Fig. 17 Effect of aluminum infiltration length on fracture mode

joints were weakened. Figure 16 shows the influence of the fracture position of the joint on tensile properties. The fracture positions of samples 1, 4, 7, 9, 12, and 13 occurred inside the rivet, and the fracture positions of samples 2, 3, 5, 6, 8, 10, and 11 occurred at the friction interface. The average values of shear strength for two fracture positions were N_{inner}=12.998 kN and N_{boundary}=12.005 kN, respectively. Therefore, the tensile properties of internal fracture of the rivet were greater than the friction interface. Figure 17 shows the effect of aluminum infiltration length on fracture modes.

The weak zones have two positions of the friction interface and the band structure. The friction interface strength is related to the degree of metallurgical bonding between the rivet and DP980. The more sufficient metallurgical bonding led to greater interface strength. The band structures were influenced by the molten aluminum penetration into the rivet. More aluminum infiltrated the rivet; more intermetallic compounds were generated inside the rivet, which weaken the overall mechanical properties. However, the metallurgical bonding and aluminum penetration were affected by the friction heating input. The higher heating input induced more sufficient metallurgical bonding, but more severe aluminum penetration.

$$N\text{inner} = \frac{\text{Gross load}}{\text{Total number}} = \frac{77.989}{6} = 12.998\ \text{kN}$$

$$N\text{boundary} = \frac{\text{Gross load}}{\text{Total number}} = \frac{84.037}{7} = 12.005\ \text{kN}$$

5 Conclusion

The friction plug-riveting spot welding solid-phase joining between AA7075 aluminum alloy and DP980 high-strength steel was performed. The morphology, mechanical properties, and fracture behavior of welded joints were revealed. Conclusions are summarized as follows:

(1) The high-strength aluminum/steel was successfully fabricated by the friction plug-riveting spot welding method. The maximum tensile shear load of the joint was 14.374 kN. The joints exhibited two fracture modes: a fracture in the rivet and a fracture in the friction interface. When the fracture mode was in the rivet, the shear load was greater than that in the friction interface.

(2) A good metallurgical bonding was formed at the interface between the rivet and DP980 steel. The interfacial reaction also occurred between the rivet and part of the aluminum alloy near the DP980 steel area, which also form a metallurgical joining, but the upper of the rivet and aluminum alloy was non-metallurgically joined.

(3) A complex thermal-mechanical interaction occurred in the zone of the rivet/steel sheet friction interface. The micro-melted aluminum alloy penetrated into the inside of the rivet. The infiltration induced the formation of a band-shaped intermetallic compound structure with a negative influence on the mechanical properties of the joint.

Author contributions Li Jianyu: preparation, creation, and presentation of the published work, specifically writing the initial draft. Liu Yajia: conducting a research, specifically performing the experiments, and data collection. Gong Shuai: construction of theoretical friction model. Chen Shuhai: acquisition of the financial support for the project leading to this publication. Huang Jihua: development or design of methodology. Chen Shujun: oversight and leadership responsibility for the research activity planning and execution. Jiang Xiaoqing: critical review, commentary, and revision

Funding The authors gratefully acknowledge financial support from the National Natural Science Foundation of China (no. 51875037).

Declarations

Conflict of interest The authors declare no competing interests.

References

1. Yang J, Oliveira JP, Li Y, Tan C, Gao C, Zhao Y, Yu Z (2022) Laser techniques for dissimilar joining of aluminum alloys to steels: a critical review. J Mater Process Technol 301:117443
2. Ma H, Qin G, Geng P, Ao Z, Chen Y (2022) Effect of intermetallic compounds on the mechanical property and corrosion behaviour of aluminium alloy/steel hybrid fusion-brazed welded structure. J Manuf Process 75:170–180
3. Li Y, Liu Y, Yang J (2020) First principle calculations and mechanical properties of the intermetallic compounds in a laser welded steel/aluminum joint. Opt Laser Technol 122:105875
4. Qiu R, Iwamoto C, Satonaka S (2009) Interfacial microstructure and strength of steel/aluminum alloy joints welded by resistance spot welding with cover plate. J Mater Process Technol 209:4186–4193
5. Azhari-Saray H, Sarkari-Khorrami M, Nademi-Babahadi A, Kashani-Bozorg SF (2020) Dissimilar resistance spot welding of 6061-T6 aluminum alloy/St-12 carbon steel using a high entropy alloy interlayer. Intermetallics 124:106876
6. Chen N, Wang H, Carlson BE, Sigler DR, Wang M (2017) Fracture mechanisms of Al/steel resistance spot welds in lap shear test. J Mater Process Technol 243:347–354
7. Karathanasopoulos N, Pandya KS, Mohr D (2021) An experimental and numerical investigation of the role of rivet and die design on the self-piercing riveting joint characteristics of aluminum and steel sheets. J Manuf Process 69:290–302
8. Abe Y, Kato T, Mori K (2009) Self-piercing riveting of high tensile strength steel and aluminium alloy sheets using conventional rivet and die. J Mater Process Technol 209:3914–3922
9. Mori K, Abe Y, Kato T (2014) Self-pierce riveting of multiple steel and aluminium alloy sheets. J Mater Process Technol 214:2002–2008
10. Karathanasopoulos N, Mohr D (2022) Strength and failure of self-piercing riveted aluminum and steel sheet joints: multi-axial experiments and modeling. J Adv Join Process 5:100107
11. Li P, Chen S, Dong H, Ji H, Li Y, Guo X, Yang G, Zhang X, Han X (2020) Interfacial microstructure and mechanical properties of dissimilar aluminum/steel joint fabricated via refilled friction stir spot welding. J Manuf Process 49:385–396
12. Chen K, Liu X, Ni J (2017) Keyhole refilled friction stir spot welding of aluminum alloy to advanced high strength steel. J Mater Process Technol 249:452–462
13. Takeoka N, Tsuchida T, Matsuda T, Ogura T, Ohashi R, Hirose A (2022) Analysis of mechanical properties of dissimilar material joint using scrubbing refill friction stir spot welding. J Adv Join Process 5:100112
14. Yu M, Zhao H, Zhang Z, Zhou L, Song X (2022) Friction surfacing assisted refilled friction stir spot welding of AA6061 alloy and Q235 steel. J Manuf Process 77:1–12
15. Huang T, Sato YS, Kokawa H, Miles MP, Kohkonen K, Siemssen B, Steel RJ, Packer S (2009) Microstructural evolution of DP980 steel during friction bit joining. Metall Mater Trans A 40:2994–3000
16. Miles MP, Kohkonen K, Packer S, Steel R, Siemssen B, Sato YS (2013) Solid state spot joining of sheet materials using consumable bit. Sci Technol Weld Joi 14:72–77
17. Miles MP, Feng Z, Kohkonen K, Weickum B, Steel R, Lev L (2013) Spot joining of AA 5754 and high strength steel sheets by consumable bit. Sci Technol Weld Joi 15:325–330
18. Lim YC, Squires L, Pan T, Miles M, Keum JK, Song G, Wang Y, Feng Z (2016) Corrosion behaviour of friction-bit-joined and weld-bonded AA7075-T6/galvannealed DP980. Sci Technol Weld Joi 22:455–464
19. Lim YC, Squires L, Pan T, Miles M, Song G, Wang Y, Feng Z (2015) Study of mechanical joint strength of aluminum alloy 7075-T6 and dual phase steel 980 welded by friction bit joining and weld-bonding under corrosion medium. Mater Des 69:37–43
20. Squires L, Lim YC, Miles MP, Feng Z (2015) Mechanical properties of dissimilar metal joints composed of DP 980 steel and AA 7075-T6. Sci Technol Weld Joi 20:242–248

Publisher's note Springer Nature remains neutral with regard to jurisdictional claims in published maps and institutional affiliations.

Springer Nature or its licensor (e.g. a society or other partner) holds exclusive rights to this article under a publishing agreement with the author(s) or other rightsholder(s); author self-archiving of the accepted manuscript version of this article is solely governed by the terms of such publishing agreement and applicable law.